Journal of the American Society for Mass Spectrometry
Research Article
Cite This: J. Am. Soc. Mass Spectrom. 2020, 31, 441−449
pubs.acs.org/jasms

Conformational Characterization of Polyelectrolyte Oligomers and Their Noncovalent Complexes Using Ion Mobility-Mass Spectrometry

Mehmet Atakay,[†] Fatma Aksakal,[†] Uğur Bozkaya,[†] Bekir Salih,*[,†] and Chrys Wesdemiotis*[,‡]

[†]Department of Chemistry, Hacettepe University, 06800 Ankara, Turkey
[‡]Department of Chemistry, The University of Akron, Akron, Ohio 44325, United States

Supporting Information

ABSTRACT: Poly-L-lysine (PLL), polystyrenesulfonate (PSS), and a mixture of these polyelectrolytes were investigated by electrospray ionization ion mobility mass spectrometry. The IM step confirmed the formation of noncovalent (i.e., supramolecular) complexes between these polyelectrolytes, which were detected in various charge states and stoichiometries in the presence of their constituents. Experimental and theoretical collision cross sections (CCSs) were derived for both PLL and PSS oligomers as well as their noncovalent assemblies. PSS chains showed higher compactness with increasing size as compared to PLL chains, indicating that the intrinsic conformations of the polyelectrolytes depend on the nature of the functional groups on their side chains. The CCS data for the noncovalent complexes further revealed that assemblies with higher PLL content have higher CCS values than other compositions of similar mass and that PLL−PSS complex formation is accompanied by significant size contraction.

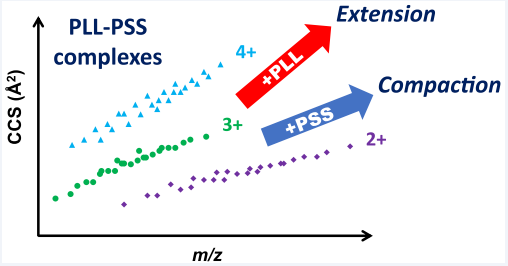

KEYWORDS: *polyelectrolyte, noncovalent complex, collision cross section, ion mobility separation, supramolecular compactness*

INTRODUCTION

Polyelectrolytes are molecules comprised of a large number of functional groups that are charged or could become charged under certain circumstances.[1−3] Their ability to interact noncovalently with oppositely charged biomolecules has led to widespread use in biomedical and sensing devices, tissue engineering, and drug delivery systems.[4−7] Polyelectrolytes are also employed as functional agents for the modification of inert material surfaces; for example, alternating layer-by-layer (LBL) deposition of positive and negative polyelectrolytes on a surface is a simple and inexpensive method for composing biocompatible, durable, and biologically relevant surfaces.[8−11]

The conformation of noncovalent polyelectrolyte complexes is a critical determinant of their properties and suitability for the above-mentioned applications. Conformational characterization of such assemblies also provides useful information for understanding interaction mechanisms in biomolecular recognition and drug/biomolecule delivery systems.[12−14] Mass spectrometry (MS) enables the identification of noncovalent complex stoichiometries with high accuracy and sensitivity, provided a soft ionization technique is used, such as electrospray ionization (ESI), which can gently transfer fragile complex structures in intact form solution (where they are formed) into the gas phase of the mass spectrometer for measurement of their masses and compositions.[15−18] Additional information about the connectivity, topology, and spatial arrangement of noncovalent assemblies can be gained by tandem mass spectrometry (MS/MS) and/or ion mobility mass spectrometry (IM-MS).[15−19] The IM-MS method[20] allows separation not only by mass and charge but also according to size and shape features, thus unveiling 3D structural detail that is difficult to obtain by other techniques from multicomponent mixtures,[21−28] especially those arising from noncovalently interacting species.[29−33] Interfacing IM-MS with the soft ionization conditions of ESI makes it possible to preserve the noncovalent interactions present in such macromolecular assemblies, so that their higher order structures can be examined.[19,29−33] In this study, ESI-IM-MS is used to characterize the conformational features of poly-L-lysine (PLL), polystyrenesulfonate (PSS), and their complexes. PLL is a cationic poly(amino acid) that is commonly used as a biomolecular carrier due to its high biocompatibility.[34−36] Conversely, PSS is a widely used polyanion in polymer and biomedical engineering due to its ability to form complexes with various types of positively charged species in a wide pH range.[37−40] The positively charged amine pendants in PLL provide an accessible interaction interface for negatively charged polyelectrolytes like PSS. Several studies have suggested that PLL−PSS complexes formed on solid materials add functionality and biocompatibility to the surfaces and also facilitate the immobilization of guest molecules on them.[41−44] IM-MS studies can divulge fundamental information about the

Received: December 17, 2019
Accepted: December 19, 2019
Published: January 3, 2020

DOI: 10.1021/jasms.9b00135
J. Am. Soc. Mass Spectrom. 2020, 31, 441−449

sizes/shapes and conformations of the polyelectrolyte complexes. This structural insight would shed light on conformational changes occurring during LBL depositions, aid structure/property correlations on the ability of polyelectrolyte complexes to capture guest molecules, and could also help to understand how polyelectrolyte films react when in contact with biological media in vivo.

EXPERIMENTAL SECTION

Materials. Poly-L-lysine (PLL) hydrobromide (mol wt 500−2000 Da), poly-DL-alanine (mol wt ∼1500−5000 Da), and all solvents were purchased from Sigma-Aldrich (St. Louis, MO). Polystyrenesulfonate (PSS) sodium salt with $M_w \approx 1100$ Da was purchased from Polymer Standards Service-USA, Inc. (Amherst, MA). All samples were used as received.

Ion Mobility Mass Spectrometry. All experiments were carried out with a SYNAPT HDMS hybrid quadrupole/time-of-flight (Q/ToF) mass spectrometer (Waters, Manchester, UK) equipped with ESI and traveling wave IM-MS capabilities. In traveling wave IM-MS, a series of continuous potential waves drives ions through a drift tube filled with an inert bath gas (typically nitrogen) flowing in the opposite direction of the ion motion.[45] Collisions between the ions with the gas slow down the ion movement. Since ions with higher collision cross section (CCS) collide more frequently with the gas, they drift more slowly through the drift tube than ions of smaller CCS. The value of CCS, which is a physical property that reflects 3D ion structure and conformation, can be derived from the corresponding measured drift time. In traveling wave IM-MS, there is no direct relationship between experimentally determined drift time and CCS; instead, CCS data are deduced by calibrating the drift time scale with standard samples of known collision cross section.[26,46,47] Singly and doubly protonated polyalanine ions were used as calibrants in this study (cf. Table S1 and Figure S7).

Solutions of PLL and PSS were prepared in water containing 30% methanol (v/v) or 10 mM ammonium acetate (NH_4OAc) containing 30% methanol (v/v) at a concentration of 0.03 mg/mL (∼0.02−0.03 mM for both polymers). Equal volumes of these solutions were mixed to form PLL−PSS complexes. The PLL, PSS, and PLL−PSS solutions were infused into the ESI source at a flow rate of 5.0 μL/min. For PLL and PLL−PSS, the solutions formed in water or NH_4OAc led to indistinguishable ESI-MS and ESI-IM-MS data in positive- or negative-ion mode. This was also true for PSS in negative-ion mode; on the other hand, only the NH_4OAc solution of PSS resulted in positive ion spectra with useable signal/noise ratio.

ESI mass spectra in positive-ion mode, ESI-MS(+), were acquired under the following settings: capillary voltage 2.5 kV, sampling cone voltage 40 V, extraction cone voltage 2.5 V, source temperature 80 °C, and desolvation gas flow rate 600 L h^{-1} (N_2) at 150 °C. The trap and transfer cell collision energy values were set at 4.0 and 6.0 eV, respectively. ESI-IM-MS(+) experiments were performed using a traveling wave height of 8.0 V, a traveling wave velocity of 350 m/s, and a IM bath gas (N_2) flow rate of 22.7 mL/min. The PLL−PSS solution was also characterized in negative ion mode by ESI-MS(−) and ESI-IM-MS(−), using the settings described in the Supporting Information. Data analysis was carried out using the MassLynx 4.1 and DriftScope 2.0 programs provided by Waters.

Calculation of Theoretical Collision Cross Sections. The semiempirical parametric method 6 (PM6) was used for geometry optimizations and harmonic vibrational frequency computations for positive ions from the compounds and complexes considered.[48] Molecular volume computations were carried out using density functional theory (DFT) at the B3LYP/6-31+G(d) level.[49−51] Grimme's third-generation dispersion correction was also applied for the noncovalent PLL−PSS complexes.[52] Theoretical CCS values in nitrogen bath gas were calculated by the hard-sphere approximation[53] using the "recommended radius" of each structure and nitrogen molecule (2.69 Å). All computations were performed with the Gaussian 09 suite of programs.[54]

RESULTS AND DISCUSSION

MS Characterization of PLL−PSS Complexes. The polyelectrolytes poly-L-lysine (PLL) and poly-(styrenesulfonate) (PSS) were initially analyzed individually by ESI-MS(+) before investigating the characteristics of their mixture. The ESI mass spectrum of PLL includes several ion distributions in the range m/z 147−659, cf. Figure S1 in the Supporting Information. The most abundant ions represent singly and doubly protonated PLL chains with H− and −OH end groups. The distance between consecutive PLL peaks is $128/n$, with 128 Da corresponding to the mass of a lysine repeating unit ($C_6H_{12}N_2O$) and n to the number of charges. Signals with low intensity resulting from either H^+/Na^+ and H^+/K^+ exchanges in the singly charged species or consecutive H_2O and NH_3 losses from the singly as well as doubly charged chains are also present in the ESI-MS spectrum. The largest PLL oligomers observed are the 5-mer with one charge (m/z 659.5) and the 6-mer with two charges (m/z 394.3). The sensitivity for detecting longer chains is significantly improved after IM separation, as documented by Figure S2, which displays the ESI mass spectrum extracted from the IM-MS region containing doubly charged PLL ions. Now, PLL chains up to 11-mer are clearly visible above noise level, along with H_2O and NH_3 losses from these oligomers. Interestingly, the extent of consecutive H_2O and NH_3 losses decreases substantially with the degree of polymerization; this trend is attributed to more extensive intramolecular hydrogen bonding in the longer chains, which evidently depresses the elimination of heteroatoms involved in such noncovalent interactions.

The PSS sample examined was supplied as the sodium salt, containing a $-SO_3Na$ moiety in each repeating unit, which promotes ionization to negative ions. When mixed with an acidic compound, a polyamine, or NH_4OAc buffer, however, PSS sodium salt undergoes extensive $-SO_3Na \rightarrow -SO_3H$ exchange and is readily ionized to positive ions as well. Figure S3 shows the ESI-MS(+) spectrum obtained from a 10 mM ammonium acetate solution. It is dominated by sodiated PSS oligomers with C_4H_9- and −H end groups and the connectivity $[C_4H_9\text{-}(C_8H_7SO_3H)_m\text{-}H + Na]^+$, ranging from the 2-mer to the 8-mer. Distributions of doubly sodiated (2+ charges) and singly ammoniated (1+ charge) ions are also observed in the mass spectrum with lower intensities. Again, using IM-MS allows to extend the detectable mass range; this is attested by the ESI-IM-MS(+) spectrum extracted from the region of doubly charged ions, which includes PSS oligomers up to 11-mer, cf. Figure S4. Mainly $[M + 2Na]^{2+}$ ions are observed, but $[M + 2NH_4]^{2+}$ and $[M + Na + NH_4]^{2+}$ species are also present in the mass spectrum, along with ions still containing one or more $-SO_3Na$ pendants ($M = C_4H_9\text{-}(C_8H_7SO_3H)_m\text{-}H$). It is noteworthy that neither PSS nor PLL form self-association products.

DOI: 10.1021/jasms.9b00135
J. Am. Soc. Mass Spectrom. 2020, 31, 441−449

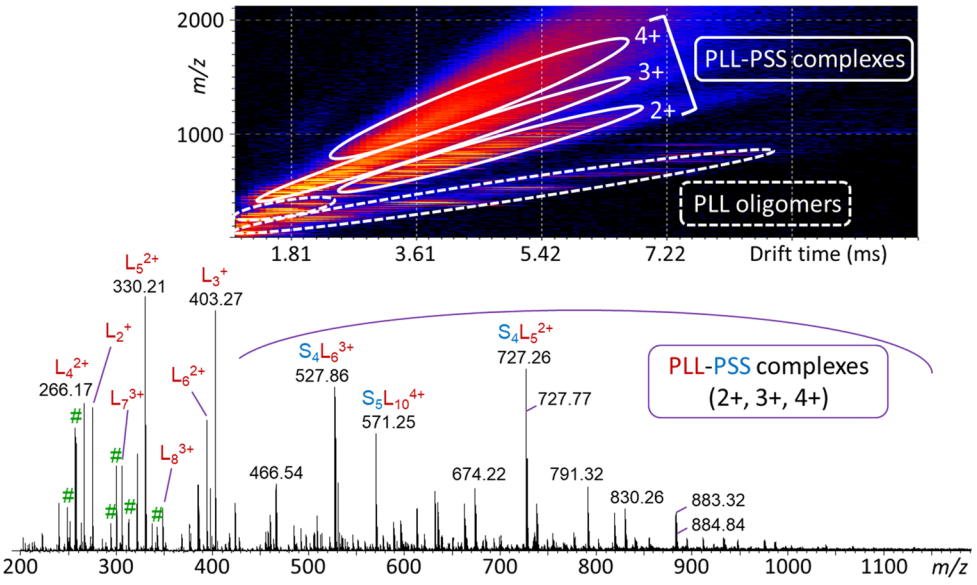

Figure 1. ESI-MS(+) spectrum of the mixture of PLL and PSS; # indicate signals corresponding to loss of water and ammonia from PLL oligomers. L = PLL repeating unit ($C_6H_{12}N_2O$); S = PSS repeating unit ($C_8H_8SO_3$). The inset shows the 2D IM-MS mobilogram (m/z vs drift time) of the PLL + PSS mixture; circled regions correspond to PLL oligomers (in various charge states) and PLL−PSS complexes in charge states 2+, 3+, and 4+.

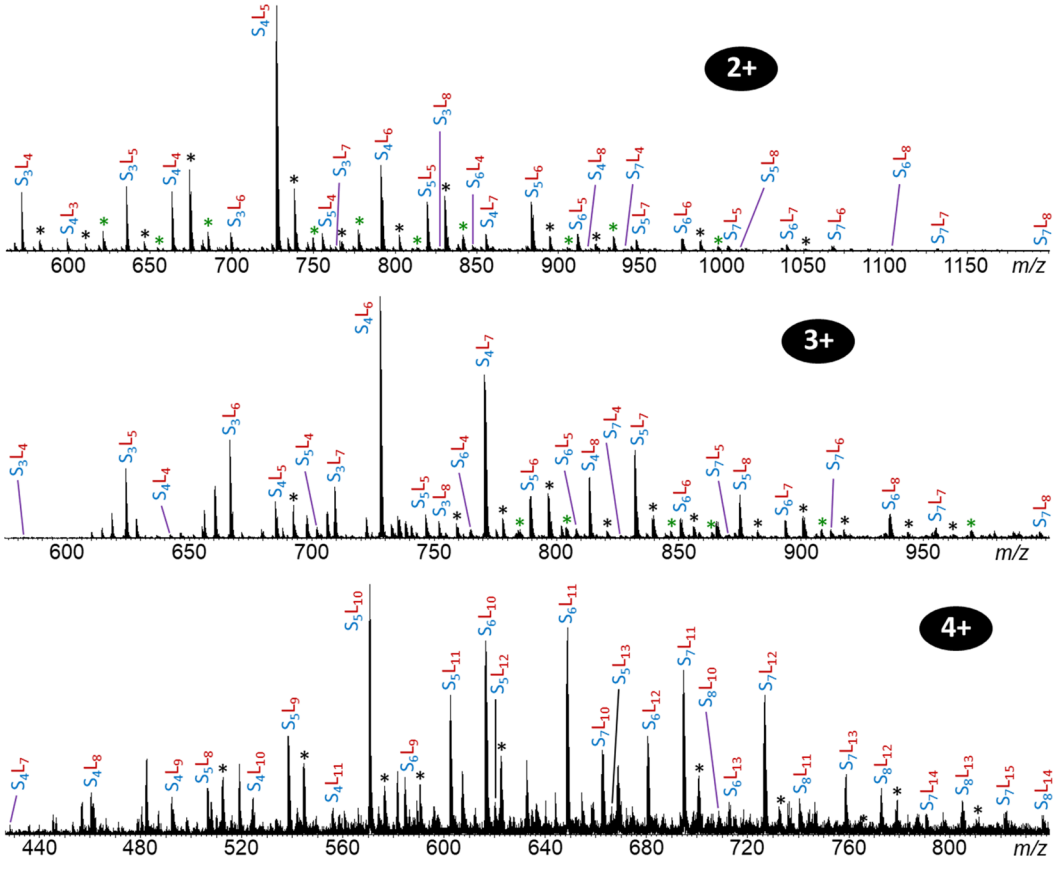

Figure 2. Mass spectra extracted from the 2D ESI-IM-MS(+) regions comprising PLL−PSS complexes in charge state 2+ (top), 3+ (center), or 4+ (bottom). Black and green asterisks indicate ions in which one or two protons, respectively, are exchanged with Na^+ ions.

Figure 1 shows the ESI-MS(+) spectrum of an approximately equimolar mixture of PLL and PSS, which includes several distributions of PLL oligomers and PLL−PSS noncovalent complexes in different charge states. This complexity is simplified, and the dynamic range significantly increased by IM-MS. The IM dimension separates by both charge state and collision cross section (CCS), spreading the ions formed upon ESI into a 2D map with well separated mobility regions for the unreacted PLL and the PLL−PSS complexes with 2+, 3+, and 4+ charges (see inset in Figure 1).

DOI: 10.1021/jasms.9b00135
J. Am. Soc. Mass Spectrom. 2020, 31, 441−449

The mass spectra extracted from the 2D ESI-IM-MS(+) regions comprising PLL−PSS complexes in charge state 2+, 3+, or 4+ are depicted in Figure 2. The noncovalent complex stoichiometries observed are labeled by S_mL_n, where S and L symbolize the PSS and PLL repeating units ($C_8H_8SO_3$ and $C_6H_{12}N_2O$, respectively), and m or n the corresponding degrees of polymerization; end groups have been omitted from this notation for brevity. The polyelectrolyte complexes are predominantly detected as $[S_mL_n + xH]^{x+}$ ions due to the extensive $-SO_3Na \rightarrow -SO_3H$ exchange occurring when PSS sodium salt is mixed with PLL in aqueous solution (vide supra). Ions that retain 1-2 Na^+ ions are also detected and have been marked by asterisks. Expectedly, complexes with longer PLL and PSS chains can accommodate more charges without destabilizing like-charge repulsion and, thus, are more abundant in higher charge states. The most abundant assemblies contain more PLL than PSS units, which makes it easier to maintain a net positive charge in the resulting complex. These trends are reflected by the dominant complex ions with 2+, 3+, and 4+ charges, which are S_4L_5, S_4L_6, and S_5L_{10}, respectively (cf. Figure 2, top to bottom).

Noncovalent PLL−PSS complexes are also detected in negative ion mode, as attested by the ESI-MS(−) spectrum in Figure S5; however, the total ion intensity is significantly lower than in positive mode. ESI-IM-MS(−) analysis further shows that the polyelectrolyte complexes form mainly $[S_mL_n - 2H]^{2-}$ along with less abundant $[S_mL_n - 3H]^{3-}$ ions, cf. Figure S6. Expectedly, the negatively charged complexes include more S than L units (i.e. a larger m/n ratio), as compared to their positively charged counterparts (Figure 1), which helps them to form more stable negative ions.

Intrinsic Conformations of PLL and PSS Oligomers. The conformational features of polyelectrolytes PLL and PSS were evaluated by measuring the collision cross sections (CCSs) of oligomers with 2+ charges and 4−11 repeating units. The CCS is a size parameter related to the averaged momentum transfer impact area of an ion as it travels through the IM chamber;[55] it reveals information about the corresponding molecular 3D geometry (conformation). IM-MS experiments provide the drift times of the traveling ions, which were converted to experimental CCS data by calibrating the drift time scale with singly and doubly protonated polyalanine oligomers of known CCS. The CCS values of the standards (N_2 buffer gas) are listed in Table S1, and the resulting calibration curve is shown in Figure S7. Using this calibration curve, the drift times of several doubly protonated PLL oligomers, viz. $[L_n + 2H]^{2+}$ (n = 4−11), and doubly sodiated PSS oligomers, viz. $[S_m + 2Na]^{2+}$ (m = 4−11), were converted to experimental CCS values, as outlined in Tables S2 and S3. The resulting data are summarized in Table 1 and agree well with CCSs predicted by theory (cf. Table 1).

Plotting the experimental CCS data vs the corresponding mass-to-charge ratios (Figure 3) unveils important information about the intrinsic (gas-phase) packing efficiency of the polyelectrolytes.[56] For the chain lengths investigated (4-mer to 11-mer, cf. Table 1), CCS increases linearly with mass for both PLL and PSS; however, the corresponding trend lines differ significantly in slope, with that of PLL (y = 0.3447x + 166.5) rising ∼50% more steeply than the trend line of PSS (y = 0.2322x + 233.05). It is evident from this trend that the intrinsic conformations of PSS oligomers become more compact with increasing degree of polymerization than those of PLL oligomers. PLL chains contain an amine group at the end of a long alkyl pendant on each repeating unit. Maximizing hydrogen bonding interactions between these side groups and between N−H protons and the backbone carbonyl groups causes the formation of expanded conformations (see computationally optimized structures of 4-mer and 11-mer in Figure 3). Meanwhile, PSS oligomers have a repeating unit with higher molecular weight; however, as seen in Figure 3, they can form more compact structures than PLL oligomers, because their repeating units can develop both electrostatic interactions (hydrogen bonding) between the sulfonate groups as well as $\pi-\pi$ interactions between the phenyl rings.

Although the PLL and PSS polyelectrolytes were ionized differently upon ESI (the former with protons and the latter with sodium ions), the conformational features discussed should be independent of the added ions and largely endowed by the distinct backbone and side chain structures of PLL vs PSS. This expectation was validated by examining doubly charged PSS containing $2NH_4^+$, a combination of $NH_4^+ + Na^+$, or $3Na^+$ (less H^+). In all cases, the CCSs are strikingly similar to those of the doubly sodiated oligomers and follow a very

Table 1. Experimental and Theoretical Collision Cross Sections of Poly-L-lysine (PLL) and Polystyrene Sulfonate (PSS) Ions with 2+ Charges

	$[L_n + 2H]^{2+}$			$[S_m + 2Na]^{2+}$		
		CCS (Å²)			CCS (Å²)	
n or m	m/z	exp[a]	theor.[b,c]	m/z	exp[a]	theor.[b,c]
4	266.20	253	267	420.07	323	298
5	330.25	281	292	512.08	349	338
6	394.30	307	314	604.09	375	340
7	457.34	323	330	696.10	400	379
8	521.39	349	362	788.11	425	410
9	586.44	373	388	880.12	448	433
10	650.49	390	400	972.13	453	435
11	714.54	408	426	1064.14	470	470

[a]Experimental collision cross section from ESI-IM-MS(+) drift times (Tables S2 and S3). [b]Theoretical collision cross section, obtained from the molecular volume computations. [c]The average difference between experimental and theoretical CCSs is 4.1 (±2.2)%.

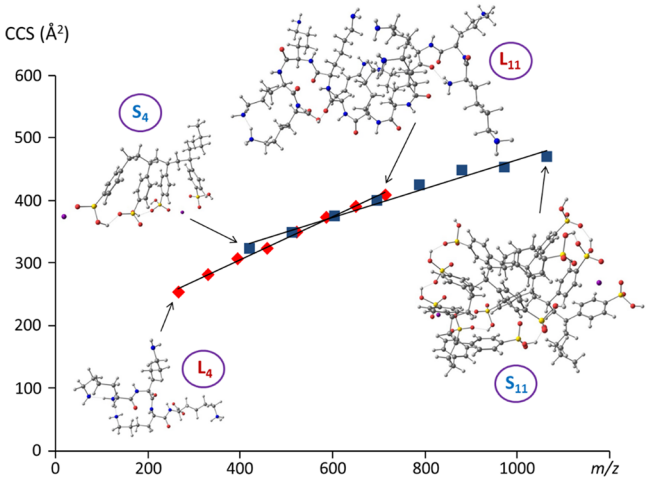

Figure 3. Plot of experimental collision cross sections vs. mass-to-charge ratios for doubly charged PLL ($[L_n + 2H]^{2+}$, n = 4-11) and PSS ($[S_m + 2Na]^{2+}$, m =4-11). PLL and PSS points are marked by ◆ and ■ signs, respectively. The insets show the computationally optimized structures of the 4-mers and 11-mers.

DOI: 10.1021/jasms.9b00135
J. Am. Soc. Mass Spectrom. 2020, 31, 441−449

similar trend line (cf. Table S4). Such finding excludes that the charge type causes the differences observed between the compactness trends of PLL vs. PSS chains (Figure 3).

Conformational Features of Noncovalent PLL−PSS Complexes. The collision cross sections derived from the IM-MS drift times of the PLL−PSS polyelectrolyte complexes in charge states 2+, 3+, and 4+ are summarized in Tables S5, S6, and S7, respectively. Additionally, plots of these experimental CCS data vs. the corresponding m/z values are depicted in Figure 4. The distribution of points in Figure 4 closely resembles the distribution of 2+, 3+, and 4+ bands in the 2D IM-MS(+) mobilogram of PLL−PSS in Figure 1, as expected.

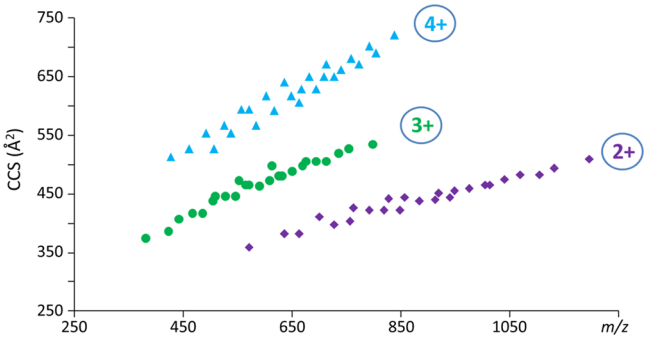

Figure 4. Plot of experimental collision cross sections vs mass-to-charge ratios for noncovalent (supramolecular) PLL−PSS complexes in charge states 2+ ($[S_mL_n + 2H]^{2+}$), 3+ ($[S_mL_n + 3H]^{3+}$), and 4+ ($[S_mL_n + 4H]^{4+}$).

For corroboration of the trends observed in the experimental CCSs of the PLL−PSS complexes, theoretical CCS values were calculated for doubly and triply protonated S_mL_n ions with m = 3−7 and n = 4−8 (mass range 1141−2389 Da). The calculated values are provided in Table 2 together with the corresponding experimental CCSs. Very good agreement between calculated and measured cross sections is observed, with the average difference between theory and experiment being 2.1 (±1.2) % for doubly protonated S_mL_n and 5.2 (±2.1)% for triply protonated S_mL_n (cf. Table 2). Note that the data in Table 2 are listed in the order of increasing n for each value of m, in order to visualize the effect in PLL vs PSS chain length, whereas the data in Tables S5−S7 are listed in the order of increasing m/z for correspondence with the plots of Figure 4.

The geometry-optimized structures of the S_mL_n complexes confirm the presence of multiple noncovalent interactions in the polyelectrolyte assemblies, both intermolecular as and intramolecular. This is exemplified in Figure 5 for doubly protonated S_3L_4, in which ion pairs (salt bridges) and hydrogen bonds connect the PLL and PSS side chains. Additionally, intrachain electrostatic interactions and $\pi-\pi$ bonding stabilize the PLL and PSS frames, respectively, resulting in a compact structure with a CCS value of 359 Å^2 (cf. Table 2).

In addition to the geometry-optimized structures described, it is possible that alternative structures with similar CCSs exist. Comprehensive calculations of the entire S_mL_n potential energy surface are, however, beyond the scope of the present study, especially since the above mentioned structures (cf. Figure 5) yield CCSs that agree very well with the measured values and observed CCS trends.

The CCSs of the PLL−PSS complexes rise in a roughly linear fashion with mass (size) according to the plots in Figure 4; however, it is obvious that certain points, especially for the doubly and triply protonated noncovalent complexes, deviate from this relationship. Complexes with a larger number of PLL units, in particular, have higher CCS values as compared to other complexes with similar mass. Likewise, complexes with lower PLL content have smaller CCS values than nearby complexes of comparable mass. These trends are more clearly recognized in Figure 6, in which the regions containing the most severely deviating points for complexes with 2+ and 3+ charges are circled and enlarged and the corresponding stoichiometries are identified.

The increased size of PLL−PSS complexes containing longer PLL chains is consistent with the CCS values and trends observed for the individual polyelectrolytes, cf. Figure 3. The $\pi-\pi$ interactions between aromatic rings of PSS, which amplify the compactness of this polymer, may be partly interrupted when a noncovalent complex with PLL is formed. This effect should be more prevalent if the PLL chain contains more repeating units than the PSS chain; indeed, S_mL_n complexes with low m/n ratio (i.e. longer PLL and shorter PSS oligomers) have relatively high CCS values, especially for overall small- to medium-sized complexes, like S_3L_6, S_3L_7, S_3L_8, and S_4L_7 with 2+ charges, or S_3L_7, S_3L_8, and S_4L_8 with 3+ charges (Figure 6). On the other hand, complexes with $m/n \approx$

Table 2. Experimental and Theoretical Collision Cross Sections of Doubly and Triply Protonated PLL−PSS Complexes

	$[S_mL_n + 2H]^{2+}$			$[S_mL_n + 3H]^{3+}$		
		CCS (Å²)			CCS (Å²)	
S_mL_n	m/z	exp[a]	theor[b,c]	m/z	exp[a]	theor[b,d]
S_3L_4	**571.27**	**359**	**359**	**381.18**	**374**	**357**
S_3L_5	635.32	381	391	423.88	385	392
S_3L_6	699.37	411	391	466.58	417	405
S_3L_7	763.41	426	437	509.28	446	420
S_3L_8	827.46	441	445	551.98	473	429
S_4L_4	**663.28**	**381**	**390**	**442.52**	**407**	**390**
S_4L_5	727.33	398	412	485.22	417	400
S_4L_6	791.38	422	433	527.92	446	432
S_4L_7	855.42	444	441	570.62	464	452
S_4L_8	919.47	451	466	613.32	497	459
S_5L_4	**755.29**	**402**	**405**	**503.86**	**437**	**413**
S_5L_5	819.34	422	429	546.56	446	436
S_5L_6	883.39	437	439	589.26	464	443
S_5L_7	947.43	455	447	631.96	481	452
S_5L_8	1011.48	465	452	674.66	504	466
S_6L_4	**847.30**	**422**	**440**	**565.20**	**464**	**423**
S_6L_5	911.35	440	454	607.90	472	456
S_6L_6	975.39	458	468	650.60	489	460
S_6L_7	1039.44	475	485	693.30	504	484
S_6L_8	1103.49	482	498	736.00	520	492
S_7L_4	**929.31**	**444**	**451**	**626.54**	**481**	**444**
S_7L_5	1003.36	465	459	669.24	497	465
S_7L_6	1067.41	482	478	711.94	504	468
S_7L_7	1131.45	494	503	754.64	527	497
S_7L_8	1195.50	510	524	797.34	534	517

[a]Experimental collision cross section from ESI-IM-MS(+) drift times (see Tables S5 and S6). [b]Theoretical collision cross section, obtained from the molecular volume computations. [c]The average difference between experimental and theoretical CCSs is 2.1 (±1.2)%. [d]The average difference between experimental and theoretical CCSs is 5.2 (±2.1)%.

DOI: 10.1021/jasms.9b00135
J. Am. Soc. Mass Spectrom. 2020, 31, 441−449

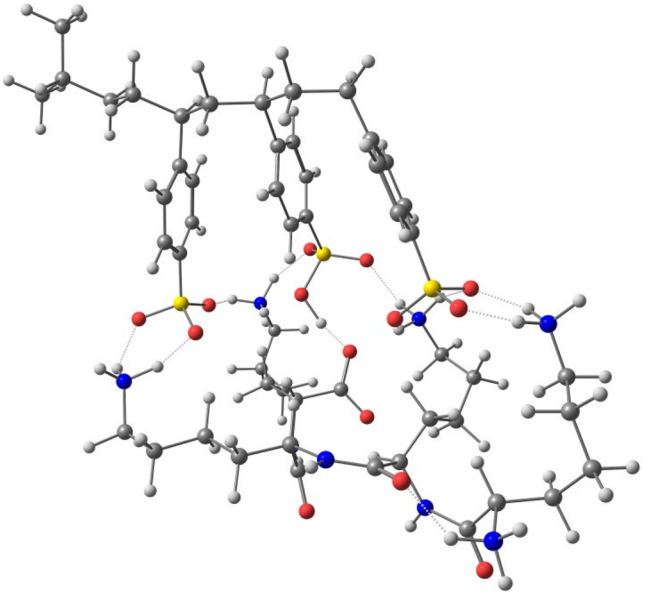

Figure 5. Geometry-optimized conformation of doubly protonated S_3L_4. Large gray, small gray, red, blue, and yellow balls represent C, H, O, N, and S atoms, respectively. The calculated CCS of this complex is 359 Å^2 (Table 2).

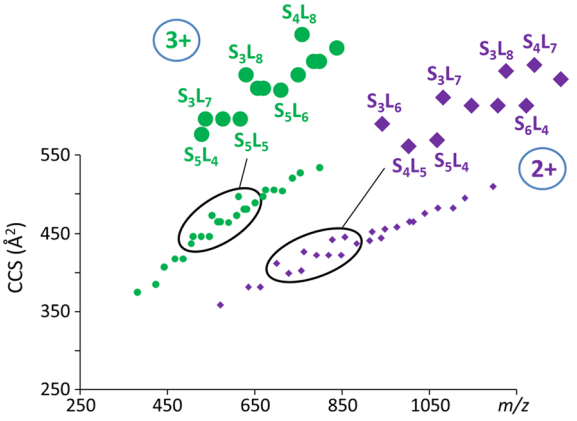

Figure 6. Plot of experimental collision cross sections vs mass-to-charge ratios for doubly and triply protonated S_mL_n complexes. The regions of highest CCS variation between adjacent points are enlarged to show the stoichiometries with particularly high or low CCS.

1 have lower CCSs than other complexes of similar m/z (cf. expanded views in Figure 6). Interestingly, fluctuations in CCS (and, hence, supramolecular size and compactness) diminish at high m/z (i.e., high $m + n$), presumably because larger complexes offer an overall greater number of sites for noncovalent intermolecular binding interactions.

Very similar trends are obtained for negatively charged PLL−PSS complexes, as attested by Figure 7 which depicts the drift times of doubly and triply deprotonated S_mL_n with m = 3−7 and n = 4−8 (cf. Tables S8−S9). CCS values were not available in this case due to the lack of appropriate calibrants; nonetheless, drift times are directly proportional to CCSs[25,56] and thus also reveal how supramolecular conformation varies with complex stoichiometry. It is evident from Figure 7 that the drift times of S_mL_n complexes with 2− and 3− charges rise in roughly linear fashion with m/z ratio; however, complexes with a higher number of PLL units (larger n) have higher drift times (and hence larger CCS values) as compared to other

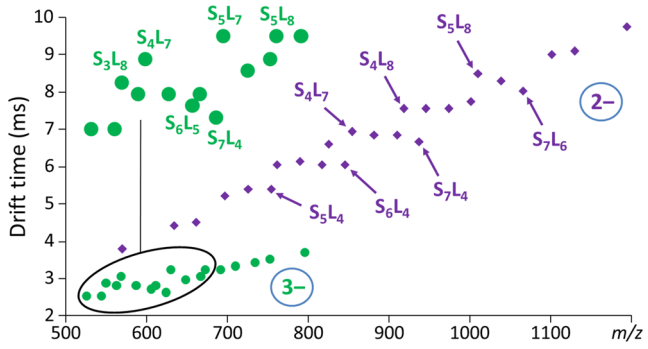

Figure 7. Plot of ESI-IM-MS(−) drift times vs mass-to-charge ratios for doubly and triply deprotonated S_mL_n complexes. The regions of highest drift time (and hence also CCS) variation between adjacent points are enlarged to show the stoichiometries with particularly high or low compactness.

complexes with similar m/z. Likewise, complexes with low PLL content have smaller drift times than nearby complexes with comparable m/z. In either charge state, compactness increases with increasing PSS content and vice versa.

Noncovalent S_mL_n complexes with longer PLL and PSS chains are mostly observed with 4+ charges (cf. Figure 2). The expanded view of the CCS vs m/z plot for this charge state (Figure 8) reveals different trends of points, depending on the

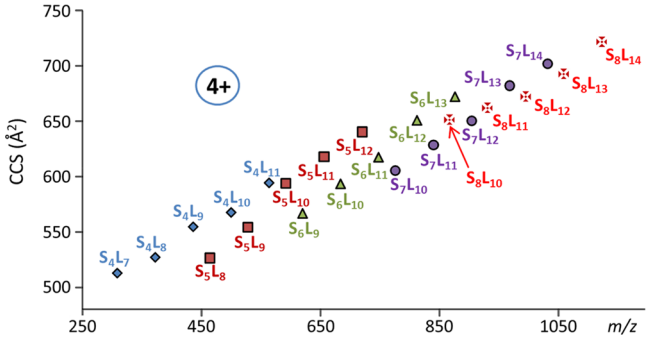

Figure 8. Expanded view of the plot of experimental collision cross sections vs mass-to-charge ratios for quadruply protonated S_mL_n complexes with m = 4−8 and n = 7−14. A different color is used for each series of complexes with the same m.

number of PSS repeating units. Due to the repulsive forces effective between like charges, conformations are generally more extended with 4+ than with 3+ or 2+ charges, as is evident from the CCS ranges in Figure 4 and Tables S5−S7; this spreads the CCS points over a larger phase space, making it easier to identify conformational trends as a function of complex stoichiometry (i.e. of m and n). In the plot of Figure 8, separate trend lines are detected for each group of PLL−PSS complexes with the same number of PSS repeating units (m fixed). Within each line, the CCS increases with increasing length of the PLL chain, corroborating that enlarging the number of PLL repeating units may obstruct size-contracting $\pi-\pi$ interactions between the aromatic rings in the PSS constituent of a complex. This assumption is supported by inspecting the CCSs of complexes with the same PLL (n fixed) but increasing PSS length; in several cases, adding a PSS repeating unit (+184 Da) barely changes the cross section, see for example S_4L_8 vs S_5L_8, S_4L_9 vs S_5L_9, S_5L_{10} vs S_6L_{10}, and S_5L_{11} vs S_6L_{11} vs. S_7L_{11}. This finding is attributed to the ability of the

DOI: 10.1021/jasms.9b00135
J. Am. Soc. Mass Spectrom. 2020, 31, 441−449

newly added PSS unit to develop not only new electrostatic interactions with PLL but also intramolecular $\pi-\pi$ interactions with other PSS units, thus balancing the increase in mass with higher compactness and minimal change in CCS.

The conformational changes taking place during supramolecular complex formation can be appraised from the CCS values of the PLL−PSS complexes (Tables 2 and S7) vs their PLL and PSS constituents (Table 1). This will be illustrated for the reaction S_4 (2+) + L_7 (2+) → S_4L_7 (4+), in which overall charge state and like-charge repelling forces for reactants and products are preserved. The combining reactants contribute CCSs of 323 Å^2 + 323 Å^2 = 646 Å^2 (cf. Table 1), while the product has a CCS of 512 Å^2 (Table S7); hence, the size shrinks by ∼21% due to the development of intermolecular and possibly new intramolecular noncovalent interactions between the oppositely charged polyelectrolyte reactants. Further, albeit smaller contractions are observed when the charge state is reduced from 4+ (512 Å^2, Table S7) to 3+ (464 Å^2, Table 2) or 2+ (444 Å^2, Table 2) due to lower repulsive forces between like charges. For the complex sizes investigated, shrinking by ∼18−25% is observed upon supramolecular assembly, with the degree of CCS reduction increasing as the difference of PLL and PSS chain lengths (i.e., $n - m$) is decreased.

CONCLUSIONS

In this study, poly-L-lysine (PLL) and polystyrene sulfonate (PSS) oligomers and their supramolecular complexes were characterized by ESI-IM-MS. The IM dimension was essential for separating and identifying the noncovalent PLL−PSS complexes in the presence of the individual polyelectrolyte reactants. Complexes with various compositions and charge states were observed, with complex stoichiometry dictating the preferred number of charges added upon ESI.

The collision cross sections of doubly charged PLL and PSS polyelectrolytes were measured in order to compare their macromolecular compactness. Intrinsic polyelectrolyte conformations were shown to depend mainly on the nature of functional groups located in the repeating units, which determine what type(s) of noncovalent bonding networks are formed.

Experimental CCS values were obtained for PLL−PSS complexes with 2+, 3+, and 4+ charges. For the lower charge states (2+, 3+), theoretical predictions were also acquired and agreed very well with the measured data in both magnitude and trends. Consistently larger sizes were found for stoichiometries rich in PLL repeating units and vice versa; this trend was also observed for PLL−PSS complexes with 2− and 3− charges.

The conformational features of larger PLL−PSS complexes with 4+ charges were also analyzed in this study. Based on their CCSs, elongating the PLL chain increases proportionally 3D conformation, whereas elongating the PSS chain causes minimal changes in 3D size, indicating that a high PSS content brings upon greater compactness.

The CCS data of the quadruply charged complexes further revealed that combining oppositely charged polyelectrolytes (PLL and PSS) leads to a significant size contraction. Further subtle changes in compactness vs. looseness can be achieved by careful adjustment of the stoichiometry of the positive vs negative polyelectrolyte chain. This information could be useful in the fabrication of polyelectrolyte multilayer films by the layer-by-layer method. In addition, the results of our study underscore the usefulness of IM-MS for the elucidation of the conformational features of synthetic polyelectrolytes and their supramolecular complexes, which may involve other synthetic polyelectrolytes (as in the present study), natural polyelectrolytes (such as proteins or oligonucleotides), and drugs or metabolites.

ASSOCIATED CONTENT

Supporting Information

The Supporting Information is available free of charge at https://pubs.acs.org/doi/10.1021/jasms.9b00135.

ESI-MS spectra, calibration plot, and tables of experimental collision cross sections and drift times (PDF)

AUTHOR INFORMATION

Corresponding Authors

*Email: wesdemiotis@uakron.edu.
*Email: bekir@hacettepe.edu.tr.

ORCID

Uğur Bozkaya: 0000-0002-5203-2210
Chrys Wesdemiotis: 0000-0002-7916-4782

Notes

The authors declare no competing financial interest.

ACKNOWLEDGMENTS

This study was supported by the National Science Foundation (CHE-1808115) and Hacettepe University (FBI-2017-13670). M.A. acknowledges the Scientific and Technological Research Council of Turkey for a doctoral research fellowship. F.A. acknowledges support from the Scientific and Technological Research Council of Turkey for a post-doctoral research fellowship (BİDEB-2218).

REFERENCES

(1) Dobrynin, A. V.; Rubinstein, M. Theory of polyelectrolytes in solutions and at surfaces. *Prog. Polym. Sci.* **2005**, *30*, 1049−1118.
(2) Uhlík, F.; Kosovan, P.; Limpouchova, Z.; Procházka, K.; Borisov, O. V.; Leermakers, F.A. Modeling of ionization and conformations of starlike weak polyelectrolytes. *Macromolecules* **2014**, *47*, 4004−4016.
(3) Meka, V. S.; Sing, M. K.; Pichika, M. R.; Nali, S. R.; Kolapalli, V. R.; Kesharwani, P. A comprehensive review on polyelectrolyte complexes. *Drug Discovery Today* **2017**, *22*, 1697−1706.
(4) Yang, X. C.; Samanta, B.; Agasti, S. S.; Jeong, Y.; Zhu, Z. J.; Rana, S.; Miranda, O. R.; Rotello, V. M. Drug delivery using nanoparticle-stabilized nanocapsules. *Angew. Chem., Int. Ed.* **2011**, *50*, 477−481.
(5) Wan, A. C.; Cutiongco, M.F.; Tai, B. C.; Leong, M. F.; Lu, H. F.; Yim, E. K. Fibers by interfacial polyelectrolyte complexation - processes, materials and applications. *Mater. Today* **2016**, *19*, 437−450.
(6) Buriuli, M.; Verma, D. Polyelectrolyte complexes (PECs) for biomedical applications. In *Advances in Biomaterials for Biomedical Applications*; Tripathi, A., Melo, J. S., Eds.; Springer: Singapore, 2017; pp 45−93.
(7) Han, Z.; Wang, Y.; Duan, X. Biofunctional polyelectrolytes assembling on biosensors - A versatile surface coating method for protein detections. *Anal. Chim. Acta* **2017**, *964*, 170−177.
(8) Decher, G. Fuzzy nanoassemblies: Toward layered polymeric multicomposites. *Science* **1997**, *277*, 1232−1237.
(9) Chluba, J.; Voegel, J. C.; Decher, G.; Erbacher, P.; Schaaf, P.; Ogier, J. Peptide hormone covalently bound to polyelectrolytes and embedded into multilayer architectures conserving full biological activity. *Biomacromolecules* **2001**, *2*, 800−805.

DOI: 10.1021/jasms.9b00135
J. Am. Soc. Mass Spectrom. 2020, 31, 441−449

(10) De Geest, B. G.; De Koker, S.; Sukhorukov, G. B.; Kreft, O.; Parak, W. J.; Skirtach, A. G.; Demeester, J.; De Smedt, S. C.; Hennink, W. E. Polyelectrolyte microcapsules for biomedical applications. *Soft Matter* **2009**, *5*, 282−291.
(11) Gribova, V.; Auzely-Velty, R.; Picart, C. Polyelectrolyte multilayer assemblies on materials surfaces: from cell adhesion to tissue engineering. *Chem. Mater.* **2012**, *24*, 854−869.
(12) Kaltashov, I. A.; Bobst, C. E.; Abzalimov, R. R.; Berkowitz, S. A.; Houde, D. Conformation and dynamics of biopharmaceuticals: transition of mass spectrometry-based tools from academe to industry. *J. Am. Soc. Mass Spectrom.* **2010**, *21*, 323−337.
(13) Du, X.; Li, Y.; Xia, Y.-L.; Ai, S.-M.; Liang, J.; Sang, P.; Ji, X.-L.; Liu, S.-Q. Insights into protein−ligand interactions: mechanisms, models, and methods. *Int. J. Mol. Sci.* **2016**, *17*, E144.
(14) Gülbakan, B.; Barylyuk, K.; Schneider, P.; Pillong, M.; Schneider, G.; Zenobi, R. Native electrospray ionization mass spectrometry reveals multiple facets of aptamer-ligand interactions: From mechanism to binding constants. *J. Am. Chem. Soc.* **2018**, *140*, 7486−7497.
(15) Loo, J. A. Studying noncovalent protein complexes by electrospray ionization mass spectrometry. *Mass Spectrom. Rev.* **1997**, *16*, 1−23.
(16) Loo, J. A. Electrospray ionization mass spectrometry: a technology for studying noncovalent macromolecular complexes. *Int. J. Mass Spectrom.* **2000**, *200*, 175−186.
(17) Rajabi, K.; Ashcroft, A. E.; Radford, S. E. Mass spectrometric methods to analyze the structural organization of macromolecular complexes. *Methods* **2015**, *89*, 13−21.
(18) Chen, F.; Gülbakan, B.; Weidmann, S.; Fagerer, S. R.; Ibáñez, A. J.; Zenobi, R. Applying mass spectrometry to study non-covalent biomolecule complexes. *Mass Spectrom. Rev.* **2016**, *35*, 48−70.
(19) Wesdemiotis, C. Multidimensional mass spectrometry of synthetic polymers and advanced materials. *Angew. Chem., Int. Ed.* **2017**, *56*, 1452−1464.
(20) Wilkins, C. L., Trimpin, S., Eds.; *Ion Mobility Spectrometry-Mass Spectrometry*; CRC Press: Boca Raton, FL, 2011.
(21) Pringle, S. D.; Giles, K.; Wildgoose, J. L.; Williams, J. P.; Slade, S. E.; Thalassinos, K.; Bateman, R. H.; Bowers, M. T.; Scrivens, J. S. An investigation of the mobility separation of some peptide and protein ions using a new hybrid quadrupole/travelling wave IMS/oa-ToF instrument. *Int. J. Mass Spectrom.* **2007**, *261*, 1−12.
(22) Harvey, S. R.; MacPhee, C.E.; Barran, P. E. Ion mobility mass spectrometry for peptide analysis. *Methods* **2011**, *54*, 454−461.
(23) Morsa, D.; Defize, T.; Dehareng, D.; Jérôme, C.; De Pauw, E. Polymer topology revealed by ion mobility coupled with mass spectrometry. *Anal. Chem.* **2014**, *86*, 9693−9700.
(24) Liu, X.; Lin, K.; Kasko, A. M.; Wesdemiotis, C. Tandem mass spectrometry and ion mobility mass spectrometry for the analysis of molecular sequence and architecture of hyperbranched glycopolymers. *Analyst* **2015**, *140*, 1182−1191.
(25) Alalwiat, A.; Grieshaber, S. E.; Paik, B. A.; Kiick, K. L.; Jia, X.; Wesdemiotis, C. Top-down mass spectrometry of hybrid materials with hydrophobic peptide and hydrophilic or hydrophobic polymer blocks. *Analyst* **2015**, *140*, 7550−7564.
(26) Alalwiat, A.; Tang, W.; Gerişlioğlu, S.; Becker, M. L.; Wesdemiotis, C. Mass spectrometry and ion mobility characterization of bioactive peptide - synthetic polymer conjugates. *Anal. Chem.* **2017**, *89*, 1170−1177.
(27) Duez, Q.; Josse, T.; Lemaur, V.; Chirot, F.; Choi, C.; Dubois, P.; Dugourd, P.; Cornil, J.; Gerbaux, P.; De Winter, J. Correlation between the shape of the ion mobility signals and the stepwise folding process of polylactide ions. *J. Mass Spectrom.* **2017**, *52*, 133−138.
(28) Dixit, S. M.; Polasky, D. A.; Ruotolo, B. T. Collision induced unfolding of isolated proteins in the gas phase: past, present, and future. *Curr. Opin. Chem. Biol.* **2018**, *42*, 93−100.
(29) Loo, J. A.; Berhane, B.; Kaddis, C. S.; Wooding, K. M.; Xie, Y.; Kaufman, S. L.; Chernushevich, I. V. Electrospray ionization mass spectrometry and ion mobility analysis of the 20S proteasome complex. *J. Am. Soc. Mass Spectrom.* **2005**, *16*, 998−1008.
(30) Uetrecht, C.; Rose, R. J.; van Duijn, E.; Lorenzen, K.; Heck, A. J. Ion mobility mass spectrometry of proteins and protein assemblies. *Chem. Soc. Rev.* **2010**, *39*, 1633−1655.
(31) Chan, Y.-T.; Li, X.; Carri, G. A.; Moorefield, C. N.; Newkome, G. R.; Wesdemiotis, C. Design, synthesis, and traveling wave ion mobility mass spectrometry characterization if iron(II)- and ruthenium(II)-terpyridine metallomacrocycles. *J. Am. Chem. Soc.* **2011**, *133*, 11967−11976.
(32) Li, X.; Chan, Y.-T.; Newkome, G. R.; Wesdemiotis, C. Gradient tandem mass spectrometry interfaced with ion mobility separation for the characterization of supramolecular architectures. *Anal. Chem.* **2011**, *83*, 1284−1290.
(33) Li, X.; Chan, Y.-T.; Casiano-Maldonado, M.; Yu, J.; Carri, G. A.; Newkome, G. R.; Wesdemiotis, C. Separation and characterization of metallosupramolecular libraries by ion mobility mass spectrometry. *Anal. Chem.* **2011**, *83*, 6667−6674.
(34) Ayyappan, J. P.; Sami, H.; Rajalekshmi, D. C.; Sivakumar, S.; Abraham, A. Immunocompatibility and toxicity studies of poly-L-lysine nanocapsules in Sprague-Dawley rats for drug-delivery applications. *Chem. Biol. Drug Des.* **2014**, *84*, 292−299.
(35) Lam, J.; Clark, E. C.; Fong, E. L.; Lee, E. J.; Lu, S.; Tabata, Y.; Mikos, A. G. Evaluation of cell-laden polyelectrolyte hydrogels incorporating poly (l-Lysine) for applications in cartilage tissue engineering. *Biomaterials* **2016**, *83*, 332−346.
(36) Kim, K.; Ryu, K.; Choi, Y. S.; Cho, Y.-Y.; Lee, J. Y.; Lee, H. S.; Kang, H. C. Effects of the physicochemical, colloidal, and biological characteristics of different polymer structures between α-poly (l-lysine) and ε-poly (l-lysine) on polymeric gene delivery. *Biomacromolecules* **2018**, *19*, 2483−2495.
(37) Rohman, G.; Huot, S.; Vilas-Boas, M.; Radu-Bostan, G.; Castner, D. G.; Migonney, V. The grafting of a thin layer of poly(sodium styrene sulfonate) onto poly(ε-caprolactone) surface can enhance fibroblast behavior. *J. Mater. Sci.: Mater. Med.* **2015**, *26*, 1−10.
(38) Yu, J.; Mao, J.; Yuan, G.; Satija, S.; Chen, W.; Tirrell, M. The effect of multivalent counterions to the structure of highly dense polystyrene sulfonate brushes. *Polymer* **2016**, *98*, 448−453.
(39) Li, N.; Hao, X.; Kang, B. H.; Li, N. B.; Luo, H. Q. Sensitive and selective turn-on fluorescence method for cetyltrimethylammonium bromide determination based on acridine orange-polystyrene sulfonate complex. *Luminescence* **2016**, *31*, 1025−1030.
(40) Shahid, S.; Gurram, S. R.; Basavaraj, M. G. Doubly pH responsive emulsions by exploiting aggregation of oppositely charged nanoparticles and polyelectrolytes. *Langmuir* **2018**, *34*, 5060−5071.
(41) Asakawa, H.; Mochitate, K.; Haruyama, T. Seamless signal transduction from live cells to an NO sensor via a cell-adhesive sensing matrix. *Anal. Chem.* **2008**, *80*, 1505−1511.
(42) Trouillon, R.; Cheung, C.; Patel, B. A.; O'Hare, D. Comparative study of poly(styrene-sulfonate)/poly(L-lysine) and fibronectin as biofouling-preventing layers in dissolved oxygen electrochemical measurements. *Analyst* **2009**, *134*, 784−793.
(43) Keller, T. F.; Müller, M.; Ouyang, W.; Zhang, J.-T.; Jandt, K. D. Templating α-helical poly(L-lysine)/polyanion complexes by nanostructured uniaxially oriented ultrathin polyethylene films. *Langmuir* **2010**, *26*, 18893−18901.
(44) Lepoitevin, M.; Jamilloux, B.; Bechelany, M.; Balanzat, E.; Janot, J.-M.; Balme, S. Fast and reversible functionalization of a single nanopore based on layer-by-layer polyelectrolyte self-assembly for tuning current rectification and designing sensors. *RSC Adv.* **2016**, *6*, 32228−32233.
(45) Giles, K.; Pringle, S. D.; Worthington, K. R.; Little, D.; Wildgoose, J.L.; Bateman, R. H. Applications of a travelling wave-based radio-frequency-only stacked ring ion guide. *Rapid Commun. Mass Spectrom.* **2004**, *18*, 2401−2414.
(46) Bush, M. F.; Hall, Z.; Giles, K.; Hoyes, J.; Robinson, C. V.; Ruotolo, B. T. Collision cross sections of proteins and their complexes: a calibration framework and database for gas-phase structural biology. *Anal. Chem.* **2010**, *82*, 9557−9565.

DOI: 10.1021/jasms.9b00135
J. Am. Soc. Mass Spectrom. 2020, 31, 441−449

(47) Bush, M. F.; Campuzano, I. D.; Robinson, C. V. Ion mobility mass spectrometry of peptide ions: effects of drift gas and calibration strategies. *Anal. Chem.* **2012**, *84*, 7124−7130.
(48) Stewart, J. J. P. Optimization of parameters for semiempirical methods V: Modification of NDDO approximations and application to 70 elements. *J. Mol. Model.* **2007**, *13*, 1173−1213.
(49) Hariharan, P. C.; Pople, J. A. The influence of polarization functions on molecular orbital hydrogenation energies. *Theor. Chim. Acta* **1973**, *28*, 213−222.
(50) Lee, C.; Yang, W.; Parr, R. G. Development of the Colle-Salvetti correlation-energy formula into a functional of the electron density. *Phys. Rev. B: Condens. Matter Mater. Phys.* **1988**, *37*, 785−789.
(51) Becke, A. D. Density-functional thermochemistry. III. *J. Chem. Phys.* **1993**, *98*, 5648−5652.
(52) Grimme, S.; Antony, J.; Ehrlich, S.; Krieg, H. A consistent and accurate ab initio parametrization of density functional dispersion correction (DFT-D) for the 94 elements H-Pu. *J. Chem. Phys.* **2010**, *132*, 154104.
(53) Shvartsburg, A. A.; Jarrold, M. F. An exact hard-spheres scattering model for the mobilities of polyatomic ions. *Chem. Phys. Lett.* **1996**, *261*, 86−91.
(54) Frisch, M. J.; Trucks, G. W.; Schlegel, H. B.; Scuseria, G. E.; Robb, M. A.; Cheeseman, J. R.; Scalmani, G.; Barone, V.; Mennucci, B.; Petersson, G. A.; Nakatsuji, H.; Caricato, M.; Li, X.; Hratchian, H. P.; Izmaylov, A. F.; Bloino, J.; Zheng, G.; Sonnenberg, J. L.; Hada, M.; Ehara, M.; Toyota, K.; Fukuda, R.; Hasegawa, J.; Ishida, M.; Nakajima, T.; Honda, Y.; Kitao, O.; Nakai, H.; Vreven, T.; Montgomery, J. A., Jr.; Peralta, J. E.; Ogliaro, F.; Bearpark, M. J.; Heyd, J.; Brothers, E. N.; Kudin, K.N.; Staroverov, V. N.; Kobayashi, R.; Normand, J.; Raghavachari, K.; Rendell, A. P.; Burant, J. C.; Iyengar, S. S.; Tomasi, J.; Cossi, M.; Rega, N.; Millam, N. J.; Klene, M.; Knox, J. E.; Cross, J. B.; Bakken, V.; Adamo, C.; Jaramillo, J.; Gomperts, R.; Stratmann, R. E.; Yazyev, O.; Austin, A. J.; Cammi, R.; Pomelli, C.; Ochterski, J. W.; Martin, R. L.; Morokuma, K.; Zakrzewski, V. G.; Voth, G. A.; Salvador, P.; Dannenberg, J. J.; Dapprich, S.; Daniels, A. D.; Farkas, Ö.; Foresman, J. B.; Ortiz, J.V.; Cioslowski, J.; Fox, D. J. Gaussian 09; Gaussian, Inc., Wallingford, CT, 2009.
(55) McDaniel, E. W.; Mason, E. A. *The Mobility and Diffusion of Ions in Gases*; Wiley: New York, 1973.
(56) Fenn, L. S.; Kliman, M.; Mahsut, A.; Zhao, S. R.; McLean, J. A. Characterizing ion mobility-mass spectrometry conformation space for the analysis of complex biological samples. *Anal. Bioanal. Chem.* **2009**, *394*, 235−244.

DOI: 10.1021/jasms.9b00135
J. Am. Soc. Mass Spectrom. 2020, 31, 441−449